



# Structure and Internal Dynamics of Short RNA Duplexes Determined by a Combination of Pulsed EPR Methods and MD Simulations

Maximilian Gauger, Marcel Heinz, Anna-Lena J. Halbritter, Lukas S. Stelzl, Nicole Erlenbach, Gerhard Hummer,\* Snorri Th. Sigurdsson,\* and Thomas F. Prisner\*

**Abstract:** We used EPR spectroscopy to characterize the structure of RNA duplexes and their internal twist, stretch and bending motions. We prepared eight 20-base-pair-long RNA duplexes containing the rigid spin-label **Çm**, a cytidine analogue, at two positions and acquired orientation-selective PELDOR/DEER data. By using different frequency bands (X-, Q-, G-band), detailed information about the distance and orientation of the labels was obtained and provided insights into the global conformational dynamics of the RNA duplex. We used <sup>19</sup>F Mims ENDOR experiments on three singly **Çm**- and singly fluorine-labeled RNA duplexes to determine the exact position of the **Çm** spin label in the helix. In a quantitative comparison to MD simulations of RNA with and without **Çm** spin labels, we found that state-of-the-art force fields with explicit parameterization of the spin label were able to describe the conformational ensemble present in our experiments. The MD simulations further confirmed that the **Çm** spin labels are excellent mimics of cytidine inducing only small local changes in the RNA structure. **Çm** spin labels are thus ideally suited for high-precision EPR experiments to probe the structure and, in conjunction with MD simulations, motions of RNA.

## Introduction

DNA and RNA form the basis for storage and transmission of genetic information in living organisms. DNA carries genetic information which is transcribed to RNA, while RNA is needed for protein biosynthesis. Apart from their function as carriers of genetic information, nucleic acids also play a crucial role in the regulation of cellular processes.<sup>[1-3]</sup> The structure and conformational dynamics of the nucleic acids are important for an understanding of their function.

Even small RNA and DNA molecules, a handful of nucleotides long, exhibit extensive dynamics, including twist-

ing and bending motions of double-stranded regions.<sup>[4-6]</sup> The nature and timescale of these conformational dynamics can vary greatly and can be broadly classified into conformational fluctuations around the equilibrium and transitions between distinct conformational states.<sup>[7,8]</sup>

Methods of structural biology like X-ray crystallography<sup>[9,10]</sup> and cryogenic electron microscopy (cryo-EM)<sup>[11-13]</sup> are well-suited to observe energetically favored individual states. Liquid state nuclear magnetic resonance (NMR) spectroscopy is another widely applied method to study conformational states of RNAs.<sup>[14,15]</sup> Typically, a representative average structure is observed due to molec-

[\*] M. Gauger, N. Erlenbach, Prof. Dr. T. F. Prisner  
 Institute of Physical and Theoretical Chemistry and Center of  
 Biomolecular Magnetic Resonance  
 Goethe University Frankfurt  
 Max-von-Laue Str. 7, 60438 Frankfurt am Main, Germany  
 E-mail: prisner@chemie.uni-frankfurt.de

M. Heinz, Prof. Dr. G. Hummer  
 Department of Theoretical Biophysics  
 Max Planck Institute of Biophysics Max-von-Laue Str. 3,  
 60438 Frankfurt am Main, Germany  
 E-mail: gerhard.hummer@biophys.mpg.de

A.-L. J. Halbritter, Prof. Dr. S. T. Sigurdsson  
 Science Institute  
 University of Iceland  
 Dunhaga 5, 107 Reykjavik, Iceland  
 E-mail: snorrishi@hi.is

L. S. Stelzl  
 Faculty of Biology  
 Johannes Gutenberg University  
 55128 Mainz, Germany

and  
 KOMET 1, Institute of Physics  
 Johannes Gutenberg University  
 Staudingerweg 9, 55128 Mainz, Germany  
 and  
 Institute of Quantitative and Computational Bioscience (IQCB)  
 Johannes Gutenberg University Mainz  
 55128 Mainz, Germany  
 and  
 Institute of Molecular Biology (IMB)  
 55128 Mainz, Germany  
 Prof. Dr. G. Hummer  
 Institute of Biophysics  
 Goethe University Frankfurt  
 Max-von-Laue Str. 1, 60438 Frankfurt am Main, Germany

© The Authors. Angewandte Chemie International Edition published by Wiley-VCH GmbH. This is an open access article under the terms of the Creative Commons Attribution Non-Commercial License, which permits use, distribution and reproduction in any medium, provided the original work is properly cited and is not used for commercial purposes.

ular tumbling and insights into the local dynamics of different domains of the biomolecule can be obtained. Under certain conditions the averaging of dipolar couplings can be partially inhibited by alignment of the sample in the magnetic field, which leads to additional insights into ensembles of structures caused by conformational fluctuations.<sup>[16–18]</sup>

EPR spectroscopy provides unique access to the structural ensembles of paramagnetically-labeled proteins and nucleic acids by resolving both thermal conformational fluctuations or multiple distinct conformational states.<sup>[19–23]</sup> A frequently used EPR method for the determination of distance constraints in the nanometer regime is pulsed electron-electron double resonance (PELDOR) spectroscopy,<sup>[24]</sup> also called double electron-electron resonance (DEER).<sup>[25]</sup> By measuring the magnetic dipolar interaction between two paramagnetic centers, distributions of distances between 1.5 and 16 nm<sup>[26]</sup> can be determined for structural ensembles, typically in frozen solution. Tikhonov regularization or other approaches are used for data analysis.<sup>[27]</sup>

To perform PELDOR experiments on nucleic acids, two paramagnetic centers need to be incorporated into the biomolecule. Typically, organic radicals, such as nitroxides<sup>[28,29]</sup> or trityls,<sup>[30,31]</sup> are synthetically incorporated at specific positions in the oligonucleotide. This provides one of the unique advantages of EPR. Since only the spin labels contribute to the detected signal, one can obtain very specific signals and, with PELDOR, specific structural information. A disadvantage is that one has to prepare multiple different labelling pairs to gain a deeper understanding of the biomolecule under investigation, which can lead to a large synthetic effort.

Concerning the spin labels, one can distinguish between flexible<sup>[32–34]</sup> and rigid spin-labels.<sup>[28,35–37]</sup> When using spin labels which are attached via flexible linkers, the flexibility resulting from rotatable bonds of the linker broadens the apparent distance distribution resulting from the conformational variety of the biomolecule. The base pairing and stacking in DNA and RNA makes it possible to introduce rigid labels, in particular the cytidine-analogue spin labels  $\zeta$ <sup>[28]</sup> for DNA and  $\zeta^m$ <sup>[35]</sup> for RNA (Figure 1, left). The radical, located at the aminoxyl (N–O) moiety, sits firmly inside the major groove of the respective B- and A-form helices (Figure 1, right).

Due to the rigidity of  $\zeta$  and  $\zeta^m$ , the distance between the two aminoxyl moieties can be determined with very high precision by PELDOR, and the distance distribution  $P(R)$  can be directly linked to the conformational flexibility of the nucleic acid itself. The rigidity also makes it possible to obtain information about the mutual orientation between the two spin labels and their orientation with respect to the interconnecting vector  $\mathbf{R}$ . This is accomplished by applying the pulses of the PELDOR experiment at specific frequency/field positions and, thereby, selecting different orientations of the anisotropic g- and A- tensors relative to the external magnetic field. These orientations are related to the orientations of the molecular frame of the spin label and are thus further related to the dipolar axis system. Such

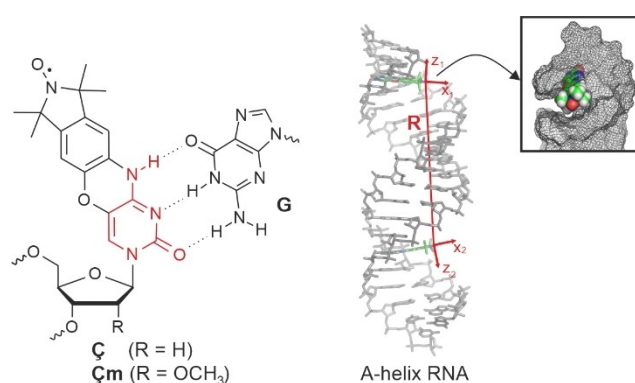


**Figure 1.** Left: The rigid spin-labels  $\zeta$  and  $\zeta^m$ . The cytosine nucleobase within the spin labels is highlighted in red. Right: Three-dimensional structure of a 20 base-pair long RNA duplex in A-helix form, doubly labeled with  $\zeta^m$  labels. The structure is taken from OL3 MD simulations where  $\zeta^m$  was explicitly parameterized. The interspin vector  $\mathbf{R}$  and the principal x- and z-axes of the spin labels are shown. Additionally, an enlarged picture of the structure of the helix around the spin label in position 3 is shown.

experiments yield orientation-dependent PELDOR time traces.

Molecular dynamics (MD) simulations are a powerful computational method for the characterization of structure and dynamics of biomolecules with atomistic resolution. MD simulations give us direct access to motions at atomistic resolution on a picosecond to microsecond timescale and can be extended in time by enhanced sampling methods. However, the simulations rest on the quality of the force fields describing the interactions. With increasing computational power and recent state-of-the-art force fields, large biological systems can be simulated, such as the nuclear pore complex,<sup>[38]</sup> or a SARS-CoV-2 virus in an aerosol droplet.<sup>[39]</sup> Nevertheless, caution is required, as small inaccuracies in the force fields become increasingly dominant with increasing system size, e.g., small non-helical RNAs and nucleic acid-protein complexes already reveal the need for force field improvements.<sup>[40,41]</sup> By contrast, for RNA and DNA in canonical duplexes, all-atom force fields such as the parm99BSC0 +  $\chi_{OL3}$ <sup>[42]</sup> (abbreviated as OL3 in this publication) and parm99BSC1,<sup>[43]</sup> respectively, already give results that are in excellent agreement with experimental data.<sup>[44,45]</sup> MD simulations with validated force fields further enable the study of highly flexible systems.<sup>[46,47]</sup>

The conformational dynamics of DNA duplexes have been investigated previously using the rigid spin-labels  $\zeta$  and orientation-selective PELDOR experiments at X- (9 GHz, 0.3 T) and G-band (180 GHz, 6.4 T). In combination with an elastic rod model, a combined twist-stretch motion with a change of the radius of the helix was postulated to be the predominant dynamic mode.<sup>[48]</sup> When combining this data with MD simulations, a more detailed picture of the internal dynamics of short DNA duplexes emerged with twist-stretch and bending motions on a nanosecond time scale.<sup>[44]</sup> The almost perfect agreement between the MD simulations using the most recent force fields, and the experimental PELDOR data also suggest that the frozen

conformational ensemble at 50 K, present in the samples used for PELDOR spectroscopy, represents the full conformational space accessible by fast internal dynamics at physiological temperatures. This has been further confirmed by room-temperature PELDOR experiments performed on an immobilized DNA duplex, which agree very well with the MD simulations when the fast nanosecond dynamics are averaged out.<sup>[49]</sup>

Here, we investigate the conformational ensemble of a 20 base-pair long RNA duplex, by preparing eight doubly- $\zeta\mathbf{m}$  labeled duplexes that cover a range of distances along the helix. Orientation-selective PELDOR experiments, in combination with MD simulations with OL3<sup>[42]</sup> and DESRES<sup>[50]</sup> force fields, gave insights into the global structure and dynamics of the RNA duplex. Building on recent successes,<sup>[51–54]</sup> we performed <sup>19</sup>F Mims ENDOR experiments to locate the exact position and orientation of the spin label in the RNA duplex and to get further insights into possible local structural variability at the site of the label in the helix. In this way the conformational ensemble of the RNA duplex was probed on a globally by PELDOR and on locally by ENDOR (Figure 1 right). We combined the PELDOR and <sup>19</sup>F Mims ENDOR experiments with atomistic OL3 MD simulations with and, for reference, without explicitly modeled spin label in the trajectory. This approach yielded a comprehensive view of the structure and motions of both the 20 base-pair RNA duplex and the spin label.

In a quantitative comparison of the experimental data to OL3 MD simulations, in which  $\zeta\mathbf{m}$  was explicitly modeled, we found that the conformations sampled by the simulations can describe the conformational ensemble present in our experiments. From the simulations, we can discern small local structural rearrangements in the vicinity of the  $\zeta\mathbf{m}$  spin label and validate the internal local dynamics of the RNA duplex motive from the quantitative agreement between EPR and MD data.

## Results and Discussion

PELDOR data were recorded at X-, Q- and G-band frequencies for eight duplex RNAs (called RNA(3,10) to RNA(3,17); numbers refer to the labeling scheme; see Supporting Information Table S2, Figure S1). First, data was obtained at Q-band frequencies (33 GHz, 1.2 T), because orientation selection can be assumed to be negligible at this frequency, since the spectral dispersion caused by the g- and A-anisotropies are on the same magnitude. This leads to a strong spectral overlap of differing orientations and therefore a negligible orientation selectivity. The distance distributions were directly obtained from the PELDOR time-traces using Tikhonov regularization (Figure S4 and S5).<sup>[55–57]</sup> Figure 2 shows the change of the mean distance (left) and the full width at half maximum (FWHM; right; determined from the half maximum of the main peak in  $P(R)$ ) with the change of the position of the second spin label for RNA (black) and DNA (yellow) duplexes. The 20 base-pair long duplex DNA samples follow the same label-

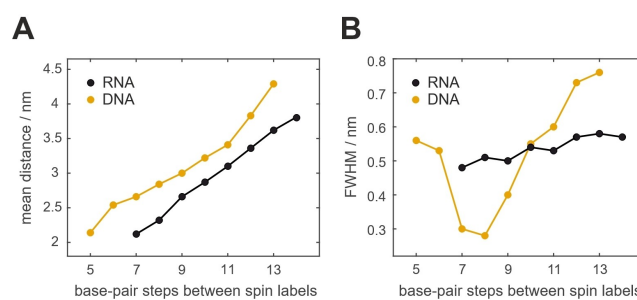


**Figure 2.** A: Mean distance as a function of the number of base-pair steps between the spin-label positions determined from PELDOR experiments on RNA (black) and DNA (yellow) duplexes with the same sequence. The RNA and DNA duplexes were doubly labeled with rigid spin-labels  $\zeta\mathbf{m}$  and  $\zeta$ , respectively. One label was fixed at the same nucleobase while the position of the second label was varied. B: Full width at half maximum (FWHM) determined from PELDOR experiments on the doubly-labeled RNA (black) and DNA (yellow) duplexes.

ing scheme as the RNA duplexes, using the spin label  $\zeta$ . The experimental data of duplex DNA were taken from Marko et al.<sup>[48]</sup> The mean distance between the spin labels measured on the RNA duplexes increases almost linearly from 2.1 nm (RNA(3,10)) to 3.8 nm (RNA(3,17)) with increasing number of base-pair steps between the spin-label positions (slope  $\sim 0.24$  nm/base-pair; Figure 2A, black line). There is a gradual increase in the FWHM of the distance distributions from 0.48 nm to 0.57 nm (Figure 2B, black line).

Interestingly, the trends between the mean distance and FWHM of RNA and DNA duplexes are different (Figure 2). While the mean distances measured in the duplex RNA increase linearly with the spacing between the labeling positions, there is a clear deviation from this trend for the duplex DNA. This can be attributed to the different geometries of the A-form RNA duplex and B-form DNA duplex and the resulting placement of the spin label pairs and their relative orientation in these different helices. The  $\zeta$  and  $\zeta\mathbf{m}$  spin labels are an extension of the cytidine nucleobase and point into the major groove of the helix. In the case of the A-helix, the major groove is shallower and enveloped by the helix backbone. In a somewhat simplified picture, the spin label points to the center of the helix (“inverted clock”, Figure 3, left). In contrast, the spin label attached to the B-helix points out into the major groove, like hands of a clock (Figure 3, right). In the case of an A-helix, there is an almost linear increase of the spin label distance as the base pair separation between the spin labels only leads to a distance change along the longitudinal helical axis. In the B-helix, this increase is modulated by an additional transversal component which depends on the angle between the tips of the spin labels (the aminoxyl moieties).

The difference between the DNA and the RNA is even more striking when comparing the FWHM trends. For the A-helix RNA there is a slight increase in FWHM as the distance between the spin labels increases, presumably because the dynamics are magnified through the length of

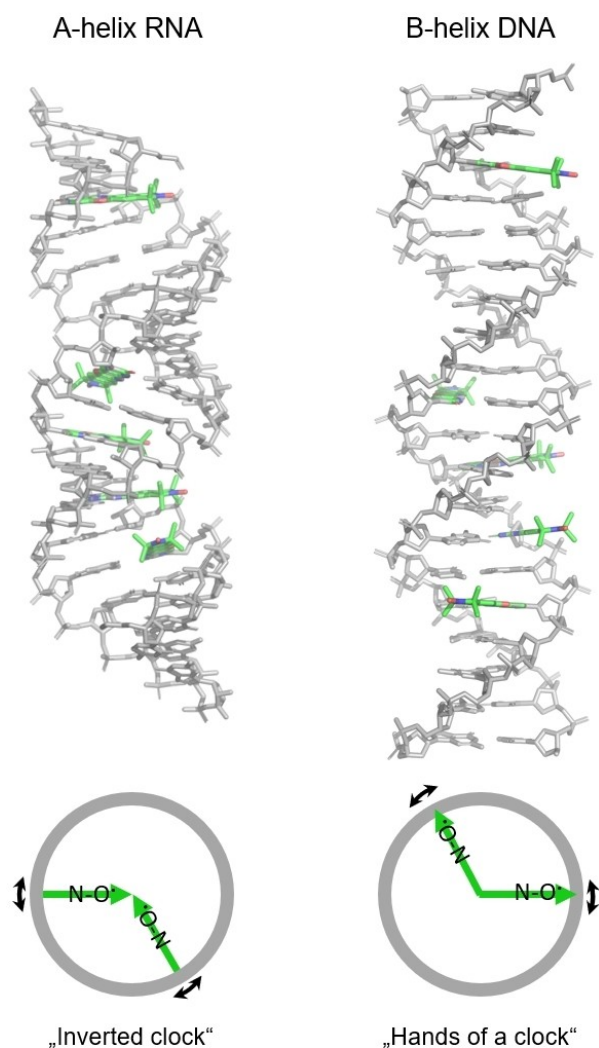


**Figure 3.** A 20 base-pair long  $\text{Cm}$ -labeled A-form RNA duplex (left) and a 20 base-pair long  $\text{C}$ -labeled B-form DNA duplex (right). Below the duplexes is a simplified representation of the spin label (green arrows) orientation within the helices viewed along the helix axis. The green arrows indicate the spin label orientations.

the helix. For the DNA duplex, the FWHM trend exhibits a clear minimum at DNA(3,11) (DNA(1,9) in the original nomenclature) and changes very strongly from one labeling position to the next. At first, one might think that the differences in these trends could indicate differences in the dynamics of A-form RNA duplexes and B-form DNA duplexes. However, this can again likely be attributed to the different geometries and resulting spin label orientations. In particular, a twist-stretch motion, which was identified as one of the main contributors to the dynamics of DNA duplexes,<sup>[44,48,58]</sup> affects the interspin distance very differently for DNA than for RNA. In an A-helix, this motion would predominantly lead to a change of the distance along the longitudinal axis of the helix, while there would be an additional transversal distance change in the B-helix DNA duplex. This transversal change would also be position-dependent and there are positions where the longitudinal and transversal changes compensate (when the labels are

close to collinear, as in DNA(3,11)). Thus, it is easier to detect differences in the interspin distances distributions caused by different types of dynamic motion in a B-form DNA duplex than in an A-form RNA duplex, using the spin labels  $\text{C}$  and  $\text{Cm}$ , respectively.

Next, we compared the Q-band PELDOR data with the duplex structures sampled by the MD simulations using the OL3 (Figure 4A, blue line) and DESRES (Figure S9) force fields. The  $\text{Cm}$  spin labels were modeled into these structures by extension of the corresponding cytidine bases with a fully rigid and linear structure of  $\text{Cm}$ .<sup>[44,59]</sup> Unexpectedly, we observed that the predicted mean distances were systematically  $\sim 0.25$  nm shorter than the experimental ones in both cases.

Considering the higher accuracy that was achieved in the comparison of PELDOR and MD simulation on  $\text{C}$  labeled duplex DNA,<sup>[44]</sup> a better agreement was expected. Errors in the MD simulation force fields are a possible reason for the discrepancy between experiment and simulation. This would mean that the global and/or local geometry of the RNA duplexes predicted by MD simulations is slightly different from the conformational ensemble in the PELDOR experiments. However, the consistency of the results for two different force fields points to other reasons. Firstly, the rigid-body superposition of the spin label onto the unlabeled RNA of the MD simulations might not be sufficiently accurate to infer the position or small inherent dynamics of the spin labels. Secondly, the incorporation of the spin label into the RNA duplex could lead to local perturbations of the RNA structure. For DNA, both possibilities have been addressed by a crystal structure of a  $\text{C}$  labeled duplex DNA, which showed the planarity and orientation of the spin label.<sup>[59]</sup>

In the absence of a crystal structure of an RNA duplex containing  $\text{Cm}$ , we decided to use  $^{19}\text{F}$  Mims ENDOR spectroscopy to determine the precise position of the spin label in the RNA duplex. We prepared three duplexes,

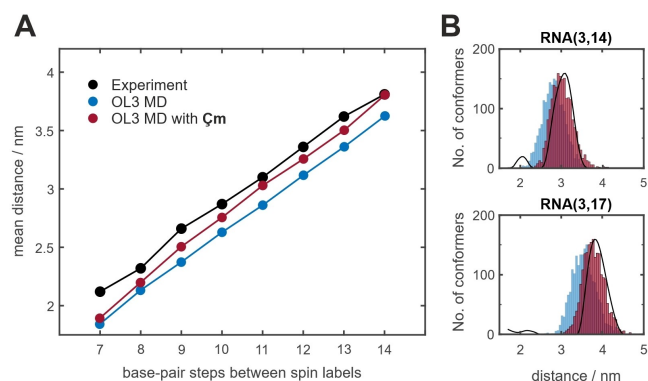


**Figure 4.** **A:** The mean interspin distance as a function of the number of base-pair steps between the spin-label positions. PELDOR experiments (black) are compared to MD simulations with the OL3 force field where the position of  $\text{Cm}$  is inferred by superimposing a rigid label onto the respective cytosine in the RNA duplex (blue) and simulations with explicitly modeled  $\text{Cm}$  labels (red). **B:** Experimental (black) and MD-simulated distance distributions (colors as in A) for RNA(3,14) (top) and RNA(3,17) (bottom).

called F6, F7, F8 (see Figure 5A), with  $\dot{\mathbf{C}}\mathbf{m}$  on one strand and a 2'-fluoro-modified nucleotide on the opposing strand. This yielded three ENDOR spectra which contain distance constraints for localizing the spin label.  $\dot{\mathbf{C}}\mathbf{m}$  was mapped onto the MD-predicted structures with the same procedure as used for the PELDOR data and the distances between the extrapolated radical position and the 2'-O-position of the ribose-backbone were used for the simulation of the  $^{19}\text{F}$  Mims ENDOR spectra. The simulated hyperfine spectra show a larger dipolar coupling than experimentally observed, leading to a broader simulated spectrum for all three samples (Figure 5B, blue line). This means that the distances between N–O and F, obtained by superimposing the label onto the unlabeled structures sampled by the MD simulations, are shorter than the experimentally-observed distances.

In contrast, the calculated and measured  $^{19}\text{F}$  Mims ENDOR spectra agree perfectly if snapshots of the MD simulations of the RNA duplex with explicitly modeled  $\dot{\mathbf{C}}\mathbf{m}$  are used (Figure 5B, red line). There is no observable difference in the simulations of the ENDOR spectra when using any of the simulations for the even labeling positions (RNA(3,10), RNA(3,12), RNA(3,14) or RNA(3,16)). This indicates a small local perturbation of the helix structure due to the the spin label in the first position, independent of the position of the second label.

Having experimentally verified by  $^{19}\text{F}$  Mims ENDOR that MD simulations of duplex RNA with explicitly modeled  $\dot{\mathbf{C}}\mathbf{m}$  accurately place the spin label within the helix, the predicted distances between the two  $\dot{\mathbf{C}}\mathbf{m}$  were compared to the PELDOR data (Figure 4, red). The MD simulations that include  $\dot{\mathbf{C}}\mathbf{m}$  yield a clear improvement and a very good agreement with the experimental PELDOR mean distance (Figure 4A, red line) and distance distribution (Figure 4B, red distributions), as compared to the MD simulations without the spin label (Figure 4, blue line and distributions). The deviation between experimental and MD-simulated mean distance is below 0.1 nm throughout the samples. For

the samples with short distances (RNA(3,10) and RNA(3,11)) the improvement is not as large as for the remaining labeling positions. This might be due to the large dipolar couplings for distances below 2 nm which are partially suppressed in our PELDOR experiments.<sup>[60]</sup>

An even more comprehensive assessment of how well the MD-generated duplex structures agree with the structural ensemble observed in our PELDOR experiments is to simulate orientation-selective PELDOR data using the spin label orientations and distances from the MD-predicted conformational ensemble. As an example, the data for RNA(3,14) and RNA(3,17) are shown in Figure 6. For these samples and throughout the entire dataset (see Figure S10 and S11), a very good agreement can be observed between the simulations from MD-predicted structures including  $\dot{\mathbf{C}}\mathbf{m}$  and the experimental data at both X- (9.4 GHz, 0.3 T) and G-band (180 GHz, 6.4 T) frequencies. Exceptions are the samples with short distances, namely RNA(3,10) and RNA(3,11), where there are still some discrepancies in the oscillation frequency. They might again result from the aforementioned suppression of short distances in experimental PELDOR time traces. As for the mean distances, a clear improvement can be observed when  $\dot{\mathbf{C}}\mathbf{m}$  is included in the MD simulations.

The experimental PELDOR time traces recorded at X- and G-band show a strong orientation selection (Figure 6, for RNA(3,14) and RNA(3,17) and Figure S6 and S7 for the other spin label positions). The orientation-dependence manifests itself in the oscillation frequency and the weighting between  $\omega_{\text{dd}}$  and  $2\omega_{\text{dd}}$  which are the dipolar frequencies expected for the interspin vector  $\mathbf{R}$  perpendicular ( $\theta=90^\circ$ ) and parallel ( $\theta=0/180^\circ$ ) to the magnetic field direction, respectively (see Equation (1);  $D_{\text{dip}} \approx 2\pi \cdot 52 \text{ MHz/nm}^3$ ). Additionally, the dampening of the oscillation, and the modulation depth ( $\Delta$ , see Figure 6) at different frequency offsets (X-band) or at different field positions (G-band) are dependent on the spin label orientations.<sup>[61–63]</sup> At X-band, the nitroxide spectrum is dominated by the z-component of

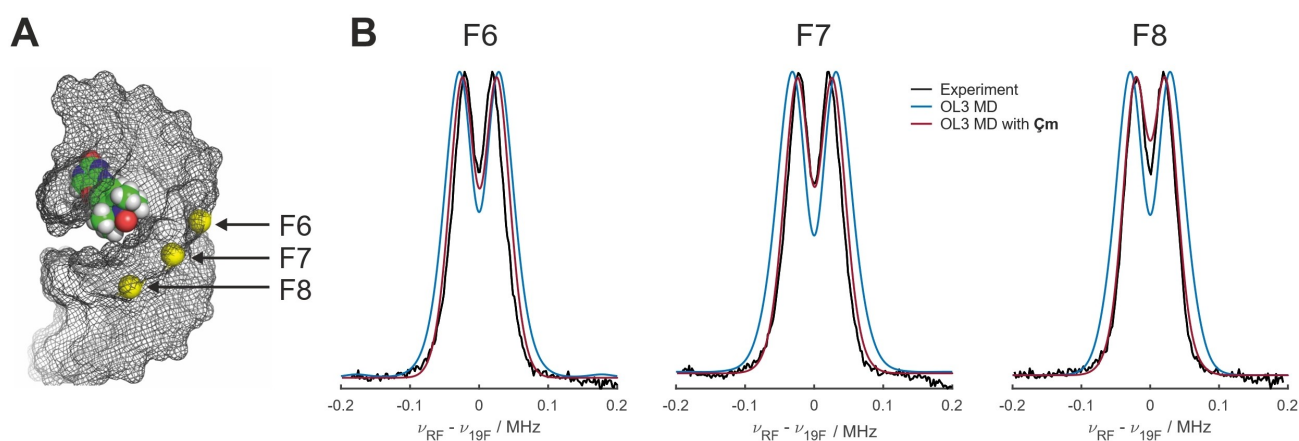


**Figure 5. A:** Structural representation of  $\dot{\mathbf{C}}\mathbf{m}$  in an A-helix RNA duplex. Three 2'-ribose positions are highlighted which show the fluorine-labeled positions. Each of the three samples, F6, F7, and F8 contains one fluorine atom and one  $\dot{\mathbf{C}}\mathbf{m}$  spin label. **B:** Experimental  $^{19}\text{F}$  Mims ENDOR spectra of samples F6 (left), F7 (middle) and F8 (right) are shown in black. Spectra simulated from OL3 MD-predicted conformers by applying a planar spin label are shown in blue. The red spectra were simulated from structures from OL3 MD simulations with explicitly modeled  $\dot{\mathbf{C}}\mathbf{m}$ .

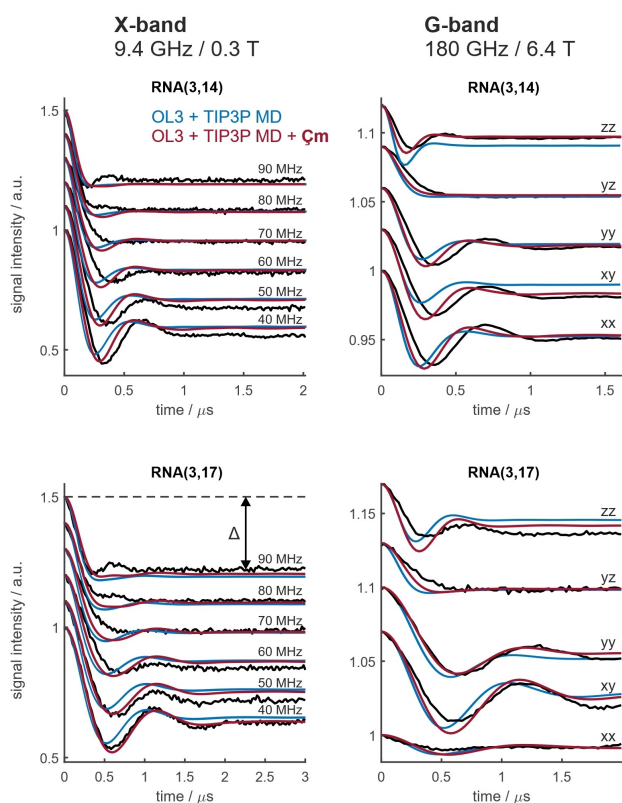


**Figure 6.** Experimental orientation-selective PELDOR data (black) recorded at X- (left) and G-band (right) shown for RNA(3,14) (top) and RNA(3,17) (bottom). The PELDOR time traces have been offset to improve legibility. Data simulated from conformers described with OL3 MD simulations where the position of  $\mathbf{\check{C}m}$  is inferred by superimposing a rigid structure of the spin label onto the respective cytosine nucleobase in the RNA duplex (blue) and MD simulations with explicitly modeled  $\mathbf{\check{C}m}$  labels (red) are shown in comparison. The modulation depth ( $\Delta$ ) is indicated in the bottom left graph.

the hyperfine tensor  $A_{zz}$ . This means that the orientation selectivity is only sensitive to changes of the orientations of the z-axes (out-of-plane axis) of the nitroxide spin labels. At G-band, due to the higher field strength, the g-anisotropy is fully resolved and, therefore, changes in the orientation of the in-plane g- and A-tensor components (x and y) additionally affect the data. This increases the complexity of the orientation-selection pattern and with that, the amount of information that can be extracted from the data. For simulations to agree well with experimental G-band data, more parameters need to be predicted correctly than for the X-band data.

$$\omega_{dip} = D_{dip} \cdot (3\cos^2\theta - 1) \cdot \frac{1}{r^3}$$

At X-band, for all labeling positions, a decrease in modulation depth was observed and an increase of the oscillation frequency with increasing frequency offset between the pump and the detection pulse sequences. The change in the oscillation frequency can be explained by the orientation of the spin labels within the RNA helix. Since, at

X-band, the nitroxide spectrum is dominated by the z-component of the hyperfine tensor ( $A_{zz}$ ), an increase of the offset between the pump pulse (in the center of the spectrum) and the detection pulses leads to an increased selection of spin label orientations where  $A_{zz}$  is parallel to the external magnetic field. Due to the helix geometry and the placement of the spin label, the N–O bond of the spin label, where the unpaired electron spin is located, is rather close to the center of the helix. Also, the normal vector of the nitroxide plane is almost parallel to the helical axis and, subsequently, the z-axis of the spin label is almost parallel to the interspin vector  $\mathbf{R}$  (Figure S2). As a consequence, for large frequency offsets, where nitroxides with  $A_{zz}$  parallel to the external field are excited, the angle  $\theta$  between the interspin vector and the external magnetic field is close to  $0^\circ$  (or  $180^\circ$ ). This leads to an oscillation frequency which is twice as high as the dipolar oscillation frequency  $\omega_{dd}$  observed at  $\theta=90^\circ$  (see Equation (1)). The decrease in modulation depth for larger frequency offsets can be explained in the same way. Because both spin labels are almost co-planar, less coupled spins can be excited by the pump pulse, which is located at the center of the nitroxide spectrum. At the offsets between 40 and 90 MHz, the  $\omega_{dd}$  and  $2\omega_{dd}$  frequency components are weighted according to the ensembles of orientations that are excited.

The shape of the oscillation (the weighting between  $\omega_{dd}$  and  $2\omega_{dd}$ ) and the dampening of the oscillation of the PELDOR time traces are reproduced well by the simulations using the OL3 MD-simulated conformer space that explicitly includes  $\mathbf{\check{C}m}$ , apart from RNA(3,10) and RNA(3,11), as discussed above (Figure 6 left, for RNA(3,14) and RNA(3,17) and Figure S10 for the other spin label positions). The MD simulations seem to slightly overestimate the conformational flexibility of the RNA duplex, as judged by stronger dampening and broader distance distributions. This could also explain the slight difference between simulation and experiment of the  $2\omega_{dd}$  component in the 90 MHz traces.

The modulation depth at different offsets is also reproduced well. The simulated set of time traces of each sample were scaled with a single factor, because the correct estimation of the absolute modulation depth is challenging and requires the exact knowledge of, e.g., the resonators' Q-factor and of homogeneous line broadening. While the microwave cavity had to be retuned for each sample, it remained unchanged while recording all time traces of one sample. Therefore, the relative modulation depth between offsets for each sample can be predicted by the orientations of the spin labels from the MD-simulated structures.

The excellent agreement between experiment and simulations from the conformational ensemble sampled by MD indicates that the magnitude and the nature of the dynamics and the accompanied variance of the interspin distance predicted by MD are in agreement with the frozen structural ensemble in the samples (see Figure 4B for a comparison of experimental and simulated distance distributions). The experimental data that were recorded at G-band also exhibit a very pronounced orientation selection (Figure 6 right, for RNA(3,14) and RNA(3,17) and Figure S7 for the other

samples). Here, both the distances between the spin centers and the orientation of the in- and out-of-plane  $g$ - and  $A$ -tensor components are encoded in the data. In agreement with the  $2\omega_{dd}$  oscillation frequency observed at 90 MHz offset at X-band, the  $2\omega_{dd}$  frequency is also observed at the  $g_{zz}$  field position where orientations of the spin label with the out-of-plane component parallel to the external magnetic field are excited. At the  $g_{xx}$  and  $g_{yy}$  field positions, the  $\omega_{dd}$  frequency component is dominant and weighted with and dampened by the  $2\omega_{dd}$  component, according to the spin label orientations present in the sample. As for the X-band data, the OL3 MD-simulated conformer space, including the modeled  $\zeta m$ , is able to reproduce the oscillation frequency and shape very well (Figure 6 right, for RNA(3,14) and RNA(3,17) and Figure S11 for the other spin label positions). We also observe that the traces calculated from MD simulated structures reproduce the relative modulation depth very well, which speaks to the high quality of the experimental data and the accuracy of the MD simulations. In particular, we highlight the observed trend of the modulation depth observed at the  $g_{xx}$  position. The modulation depth at this position is proportional to the angle between the x-axes of both spin labels. The trend follows the expected periodicity derived from the geometry of the double-helical structure of RNA very nicely and is reproduced perfectly by the MD simulations (Figure S12). The maximum modulation depth occurs for RNA(3,14) with 11 base pairs difference, where the spin labels are almost collinear to each other, in excellent agreement with the MD simulations.

To visualize the differences between the MD simulations of the RNA duplex with and without the spin labels, we compared the distributions of a few helical parameters around the spin labeled site to other parts of the helix. The parameters were extracted and processed using the software package 3DNA.<sup>[64,65]</sup> The following parameters were chosen: helical twist (angle between consecutive base pairs), helical rise (distance along the helix between consecutive base pairs), inclination (angle between base pair and helical axis), propeller angle (angle between the planes of the nucleobase rings in a base pair) and helix radius (calculated from the C1' positions). The twist, rise and radius reflect the global structure of the RNA duplex and its conformational variety, while variation of the inclination and propeller angle reflects local changes in the RNA duplex. The propeller twist is of special interest here as  $\zeta m$  is an extension of the C nucleobase and, therefore, the distance and orientation of the spin labels are strongly influenced by changes in this parameter. When comparing the distributions of our chosen parameters for the entire sequence of the predicted structures from the MD simulations of the labeled and unlabeled RNA helix, some differences can be observed (Figure S15) which will be discussed in the following paragraphs.

The unmodified helical section, between the two spin labeled sites, and the section in the immediate vicinity of the spin label were evaluated separately to understand extent of the structural changes induced by  $\zeta m$ . The unmodified helical section of the MD simulation with explicitly modeled

$\zeta m$ , shows no difference to the simulations of the corresponding unlabeled RNA duplex (Figure 7, left). Both the distributions of the selected helical parameters and the average structures of the MD trajectories aligned on the unmodified section look identical. The values we observe are in agreement with other MD simulations of GC-rich RNA duplexes.<sup>[66]</sup>

The parameter distributions change noticeably when looking at the part of the helix around the spin labeled position ( $\pm 2$  base pairs around the label; Figure 7, right). The first obvious and local change is an increase of the base-pair propeller angle, which affects the interspin distance. If the nucleobase twists and, in this case, the base pair becomes flatter, a longer distance is obtained. Interestingly, the propeller twist of labeled base pairs (base pair 3 and 14 for RNA(3,14)) seems virtually unchanged. The changes contributing to the shift in the distribution upon incorporation of the spin label introduction seem to occur at the unlabeled base pairs around the labeled base pair. All parameters together, including the helical twist, rise, and radius (Figure 7), imply a partial unwinding of the helix. As the helix widens and stretches (increase of the radius and helical rise respectively), the twist and inclination angle decrease. This

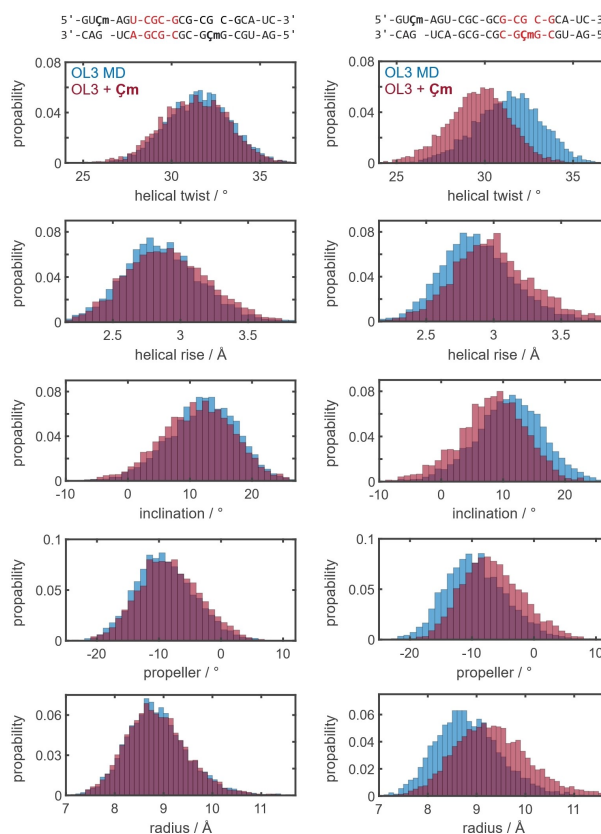


**Figure 7.** Changes in helix parameters when including  $\zeta m$  in the MD simulations. The distribution of the helical twist, rise, inclination, propeller angle and radius are shown for five base pairs between the spin labels at position 3 and 14 (base pairs 6 to 10; left) and  $\pm 2$  base pairs around the spin label at position 14 (base pairs 12 to 16; right). Data are shown for the unlabeled (blue) and labeled (red; RNA(3,14)) OL3 MD simulations.

results in a wider, slightly unwound section of the helix, with more base pairs per turn (Figure 7, right). These local changes are confined to  $\pm 2$  base pairs around the label position and manifest as a partial opening of the major and minor grooves of the helix. The opening of the grooves around the spin labeled positions leads to a slight elongation of the labeled duplex as compared to the unlabeled duplex. In spite of these local changes, there is no perceivable difference in the helix dynamics between the labeled and the unlabeled duplexes when looking at the helix motions, i.e., the principal components. The dynamics present in the first three principal components are a convolution of a helical bending and twist-stretch (winding/unwinding) motion. The first two principal components are dominated by a bending motion while the third is dominated by twist-stretching.

The spin label exhibits some dynamics of its own during the MD simulation. The flexibility of the oxazine linker is the largest contributor to these dynamics. The angle between the five-membered ring and the nucleobase varies around  $10^\circ$  ( $\sigma$ ) in either direction with a slight preference of the spin labels bending towards each other ( $\sim 3.2^\circ$  throughout all labeling positions; Figure S18). However, the effect of the spin label flexibility on the width of the distance distribution is small, compared to the changes caused by the helix dynamics (Figure S19). The **C** and **Cm** spin labels can, therefore, in good conscience be called rigid labels and offer the advantage of more precise distance measurements, compared to flexible spin labels. Only the well-structured nature of the 20 base-pair RNA duplex in combination with the rigid label **Cm** made it possible to resolve the position of **Cm** in the major groove of the duplex to the accuracy shown here. For more complex and flexible structures, these details would likely be obscured by additional large global dynamics of the biomolecule.

## Conclusion

The aim of this study was to investigate the conformational dynamics of helical regions in duplex RNA with PELDOR and orientation-selective PELDOR experiments, using a 20 base-pair long construct that was doubly labeled with the rigid spin-label **Cm** at different positions along the sequence.  $^{19}\text{F}$  Mims ENDOR data recorded on the same RNA duplex construct as used for the PELDOR experiments gave additional insights into the local helical structure and the exact position of the spin label in the major groove of the RNA helix. To aid in the interpretation of the experimental data and for an atomistic insight into the structure and dynamics of RNA duplexes, we performed MD simulations in the absence and presence of the spin label. The result was a helical structure that is close to a standard A-form RNA helix and undergoes dynamics which are dominated by bending and winding/unwinding (twist-stretch) motions. There are some deviations from the reference A-form helices (in particular the radius) which are not surprising due to the high GC content in the sequence of the duplex.

While the predicted structural ensemble from MD simulations of the RNA duplex without explicit spin labels

yields a qualitative impression of the dynamics of the RNA duplex, it does not yield a quantitative agreement with our experimental data. A deviation of around 0.25 nm was observed in the mean spin label distance.

However, when the spin label is explicitly modeled and simulated within the duplex RNAs, a perfect agreement with the ENDOR data (local geometry/dynamics) was observed and a much better agreement with the PELDOR distance and orientation predictions (global structure/dynamics) was achieved.

The major factor contributing to the improvement is a small local structural rearrangement of the helix in the region  $\pm 2$  base pairs around the spin labeled site: a slight opening or unwinding of the helix close to the spin labeled position. The overall helix dynamics are conserved with or without the spin label. The small local rearrangements we were able to resolve here, will also likely not change additional large-scale dynamics of more flexible RNA.

The advantage of the approach presented here is that the conformational ensemble can be investigated on the local (ENDOR) and global (PELDOR) scale on a very similar construct in the same sample environment. The MD simulations aid in the understanding of the experimental data and pinpoint small local structural around the labeled positions.

Overall, we could show how **Cm** is positioned in a duplex RNA helix and resolved small local structural rearrangements by combining  $^{19}\text{F}$  ENDOR, long-distance and orientation-selective measurements from PELDOR experiments and a quantitative comparison with MD simulations.

We want to emphasize the synergy between EPR experiments and MD simulations that will enable further investigation of the structure and dynamics of nucleic acids with rigid spin labels. This could include nucleic acids that contain non-canonical elements, e.g., non-Watson-Crick base pairs, base-pair mismatches or bulges. Moreover, it may be possible to study sequence-dependent structural variations, related to function, with this approach. Also, extending and adapting this approach to more flexible RNA motifs, such as stem loops or aptamers with more complex tertiary structures and dynamics will be of great interest.

## Acknowledgements

The three-dimensional nucleic acid structures were visualized with the open-source software PyMOL. M.G., T.F.P., A.-L.J.H. and S.Th.S. acknowledge financial support from the Collaborative Research Center 902 (Molecular Principles of RNA-based regulation) of the German Research Foundation (3214020004). A.-L.J.H., S.Th.S. acknowledge financial support from the Icelandic Research Fund (206708). M.H. and G.H. were supported by the German Federal Ministry of Education and Research (BMBF, Cluster4Future, Proxidrugs) and by the Max Planck Society. L.S.S. thanks ReALity (Resilience, Adaptation and Longevity), M3ODEL (Mainz Institute of Multiscale Modeling) and Forschungsinitiative des Landes Rheinland-Pfalz for

their support. Open Access funding enabled and organized by Projekt DEAL.

### Conflict of Interest

The authors declare no conflict of interest.

### Data Availability Statement

The data that support the findings of this study are available from the corresponding author upon reasonable request.

**Keywords:** EPR spectroscopy · molecular dynamics · RNA · PELDOR spectroscopy · ENDOR spectroscopy

- [1] R. Rohs, X. Jin, S. M. West, R. Joshi, B. Honig, R. S. Mann, *Annu. Rev. Biochem.* **2010**, *79*, 233–269.
- [2] D. P. Bartel, *Cell* **2009**, *136*(2), 215–233.
- [3] R. R. Breaker, *Cold Spring Harbor Perspect. Biol.* **2012**, *4*(2).
- [4] C. Bustamante, Z. Bryant, S. B. Smith, *Nature* **2003**, *421*(6921), 423–427.
- [5] A. Pérez, A. Noy, F. Lankas, F. J. Luque, M. Orozco, *Nucleic Acids Res.* **2004**, *32*(20), 6144–6151.
- [6] J. F. Marko, E. D. Siggia, *Macromolecules* **1994**, *27*(4), 981–988.
- [7] E. A. Dethoff, J. Chugh, A. M. Mustoe, H. M. Al-Hashimi, *Nature* **2012**, *482*(7385), 322–330.
- [8] H. M. Al-Hashimi, N. G. Walter, *Curr. Opin. Struct. Biol.* **2008**, *18*(3), 321–329.
- [9] E. Ennifar, *1st editio., Ennifar, E., Ed., Methods in Molecular Biology*, Springer New York: New York, NY, **2016**, Vol. 1320.
- [10] B. S. Schuwirth, M. A. Borovinskaya, C. W. Hau, W. Zhang, A. Vila-Sanjurjo, J. M. Holton, J. H. D. Cate, *Science* **2005**, *310*(5749), 827–834.
- [11] M. Topf, K. Lasker, B. Webb, H. Wolfson, W. Chiu, A. Sali, *Structure* **2008**, *16*(2), 295–307.
- [12] X.-c. Bai, T. G. Martin, S. H. W. Scheres, H. Dietz, *Proc. Nat. Acad. Sci.* **2012**, *109*(49), 20012–20017.
- [13] F. Tama, M. Valle, J. Frankt, C. L. Brooks, *Proc. Natl. Acad. Sci. USA* **2003**, *100*(16), 9319–9323.
- [14] B. Fürtig, C. Richter, J. Wöhnert, H. Schwalbe, *ChemBioChem* **2003**, *4*(10), 936–962.
- [15] J. R. Bothe, E. N. Nikolova, C. D. Eichhorn, J. Chugh, A. L. Hansen, H. M. Al-Hashimi, *Nat. Methods* **2011**, *8*(11), 919–931.
- [16] A. Saupe, G. Englert, *Phys. Rev. Lett.* **1963**, *11*(10), 462–464.
- [17] J. W. Emsley, J. C. Lindon, First edit., Pergamon Press, **1975**.
- [18] J. H. Prestegard, H. M. Al-Hashimi, J. R. Tolman, *Q. Rev. Biophys.* **2000**, *33*(4), 371–424.
- [19] O. Schiemann, A. Weber, T. E. Edwards, T. F. Prisner, S. T. Sigurdsson, *J. Am. Chem. Soc.* **2003**, *125*(12), 3434–3435.
- [20] O. Schiemann, T. F. Prisner, *Q. Rev. Biophys.* **2007**, *40*(1), 1–53.
- [21] P. Z. Qin, K. Hideg, J. Feigon, W. L. Hubbell, *Biochemistry* **2003**, *42*(22), 6772–6783.
- [22] G. Jeschke, Y. Polyhach, *Phys. Chem. Chem. Phys.* **2007**, *9*(16), 1895.
- [23] V. P. Denysenkov, D. Biglino, W. Lubitz, T. F. Prisner, M. Bennati, *Angew. Chem. Int. Ed.* **2008**, *47*(7), 1224–1227.
- [24] A. D. Milov, K. M. Slikhov, M. D. Shirov, *Fiz. Tverd. Tela* **1981**, *23*, 975.
- [25] R. G. Larsen, D. J. Singel, *J. Chem. Phys.* **1993**, *98*(7), 5134–5146.
- [26] T. Schmidt, M. A. Wälti, J. L. Baber, E. J. Hustedt, G. M. Clore, *Angew. Chem. Int. Ed.* **2016**, *55*(51), 15905–15909.
- [27] O. Schiemann, C. A. Heubach, D. Abdullin, K. Ackermann, M. Azarkh, E. G. Bagryanskaya, M. Drescher, B. Endeward, J. H. Freed, L. Galazzo, D. Goldfarb, T. Hett, L. Esteban Hofer, L. Fábregas Ibáñez, E. J. Hustedt, S. Kucher, I. Kuprov, J. E. Lovett, A. Meyer, S. Ruthstein, S. Saxena, S. Stoll, C. R. Timmel, M. Di Valentin, H. S. McHaourab, T. F. Prisner, B. E. Bode, E. Bordignon, M. Bennati, G. Jeschke, *J. Am. Chem. Soc.* **2021**, *143*(43), 17875–17890.
- [28] N. Barhate, P. Cekan, A. P. Massey, S. T. Sigurdsson, *Angew. Chem. Int. Ed.* **2007**, *46*(15), 2655–2658.
- [29] S. A. Shelke, S. T. Sigurdsson, *Angew. Chem. Int. Ed.* **2010**, *49*(43), 7984–7986.
- [30] G. Y. Shevelev, O. A. Krumkacheva, A. A. Lomzov, A. A. Kuzhelev, D. V. Trukhin, O. Y. Rogozhnikova, V. M. Tormyshev, D. V. Pyshnyi, M. V. Fedin, E. G. Bagryanskaya, *J. Phys. Chem. B* **2015**, *119*(43), 13641–13648.
- [31] N. Fleck, C. A. Heubach, T. Hett, F. R. Haege, P. P. Bawol, H. Baltruschat, O. Schiemann, *Angew. Chem.* **2020**, *132*(24), 9854–9859.
- [32] Q. Cai, A. K. Kusnetzow, W. L. Hubbell, I. S. Haworth, G. P. C. Gacho, N. Van Eps, K. Hideg, E. J. Chambers, P. Z. Qin, *Nucleic Acids Res.* **2006**, *34*(17), 4722–4730.
- [33] T. E. Edwards, S. T. Sigurdsson, *Nat. Protoc.* **2007**, *2*(8), 1954–1962.
- [34] M. Kerzhner, D. Abdullin, J. Więcek, H. Matsuoka, G. Hagelueken, O. Schiemann, M. Famulok, *Chem. A Eur. J.* **2016**, *22*(34), 12113–12121.
- [35] C. Höbartner, G. Sicoli, F. Wachowius, D. B. Gophane, S. T. Sigurdsson, *J. Org. Chem.* **2012**, *77*(17), 7749–7754.
- [36] A. L. J. Segler, S. T. Sigurdsson, *J. Org. Chem.* **2021**, *86*(17), 11647–11659.
- [37] L. M. Stratmann, Y. Kutin, M. Kasanmascheff, G. H. Clever, *Angew. Chem. Int. Ed.* **2021**, *60*(9), 4939–4947.
- [38] S. Mosalaganti, A. Obarska-Kosinska, M. Siggel, R. Taniguchi, B. Turoňová, C. E. Zimmerli, K. Buczak, F. H. Schmidt, E. Margiotta, M.-T. Mackmull, W. J. H. Hagen, G. Hummer, J. Kosinski, M. Beck, *Science* **2022**, *376*(6598).
- [39] A. Dommer, L. Casalino, F. Kearns, M. Rosenfeld, N. Wauer, S. H. Ahn, J. Russo, S. Oliveira, C. Morris, A. Bogetti, A. Trifan, A. Brace, T. Sztain, A. Clyde, H. Ma, C. Chennubhotla, H. Lee, M. Turilli, S. Khalid, T. Tamayo-Mendoza, M. Welborn, A. Christensen, D. G. A. Smith, Z. Qiao, S. K. Sirumalla, M. O'Connor, F. Manby, A. Anandkumar, D. Hardy, J. Phillips, A. Stern, J. Romero, D. Clark, M. Dorrell, T. Maiden, L. Huang, J. McCaLpin, C. Woods, A. Gray, M. Williams, B. Barker, H. Rajapaksha, R. Pitts, T. Gibbs, J. Stone, D. M. Zuckerman, A. J. Mulholland, T. Miller, S. Jha, A. Ramanathan, L. Chong, R. E. Amaro, *Int. J. High Perform. Comput. Appl.* **2023**, *37*(1), 28–44.
- [40] K. Mráziková, V. Mlýnský, P. Kührová, P. Pokorná, H. Kruse, M. Krepl, M. Otyepka, P. Banáš, J. Šponer, *J. Chem. Theory Comput.* **2020**, *16*(12), 7601–7617.
- [41] P. Pokorná, M. Krepl, S. Campagne, J. Šponer, *J. Phys. Chem. B* **2022**, *126*(45), 9207–9221.
- [42] M. Zgarbová, M. Otyepka, J. Šponer, A. Mládek, P. Banáš, T. E. Cheatham, P. Jurečka, *J. Chem. Theory Comput.* **2011**, *7*(9), 2886–2902.
- [43] I. Ivani, P. D. Dans, A. Noy, A. Pérez, I. Faustino, A. Hospital, J. Walther, P. Andrio, R. Goñi, A. Balaceanu, G. Portella, F. Battistini, J. L. Gelpí, C. González, M. Vendruscolo, C. A. Lughton, S. A. Harris, D. A. Case, M. Orozco, *Nat. Methods* **2016**, *13*(1), 55–58.

- [44] L. S. Stelzl, N. Erlenbach, M. Heinz, T. F. Prisner, G. Hummer, *J. Am. Chem. Soc.* **2017**, *139*(34), 11674–11677.
- [45] P. Kührová, V. Mlýnský, M. Otyepka, J. Šponer, P. Banáš, *J. Chem. Inf. Model.* **2023**, *63*(7), 2133–2146.
- [46] K. K. Grotz, M. F. Nueesch, E. D. Holmstrom, M. Heinz, L. S. Stelzl, B. Schuler, G. Hummer, *J. Phys. Chem. B* **2018**, *122*(49), 11626–11639.
- [47] Z. Zhang, J. Šponer, G. Bussi, V. Mlýnský, P. Šulc, C. R. Simmons, N. Stephanopoulos, M. Krepl, *J. Chem. Inf. Model.* **2023**, *63*(9), 2794–2809.
- [48] A. Marko, V. Denysenkov, D. Margraf, P. Cekan, O. Schiemann, S. T. Sigurdsson, T. F. Prisner, *J. Am. Chem. Soc.* **2011**, *133*(34), 13375–13379.
- [49] M. Gränz, N. Erlenbach, P. Spindler, D. B. Gophane, L. S. Stelzl, S. T. Sigurdsson, T. F. Prisner, *Angew. Chem. Int. Ed.* **2018**, *57*(33), 10540–10543.
- [50] D. Tan, S. Piana, R. M. Dirks, D. E. Shaw, *Proc. Nat. Acad. Sci.* **2018**, *115*(7), E1346–E1355.
- [51] A. Meyer, S. Dechert, S. Dey, C. Höbartner, M. Bennati, *Angew. Chem. Int. Ed.* **2020**, *59*(1), 373–379.
- [52] N. B. Asanbaeva, A. A. Sukhanov, A. A. Diveikina, O. Y. Rogozhnikova, D. V. Trukhin, V. M. Tormyshev, A. S. Chubarov, A. G. Maryasov, A. M. Genaev, A. V. Shernyukov, G. E. Salnikov, A. A. Lomzov, D. V. Pyshnyi, E. G. Bagryan-skaya, *Phys. Chem. Chem. Phys.* **2022**, *24*(10), 5982–6001.
- [53] M. Seal, W. Zhu, A. Dalaloyan, A. Feintuch, A. Bogdanov, V. Frydman, X. Su, A. M. Gronenborn, D. Goldfarb, *Angew. Chem. Int. Ed.* **2023**, *62*(20), e202218780.
- [54] S. L. Schumann, S. Kotnig, Y. Kutin, M. Drosou, L. M. Stratmann, Y. Streltsova, A. Schnegg, D. A. Pantazis, G. H. Clever, M. Kasanmascheff, *Chem. A Eur. J.* **2023**, *202302527*, 1–8.
- [55] A. N. Tikhonov, *Dokl. Akad. Nauk* **1963**, *151*, 501.
- [56] Y.-W. Chiang, P. P. Borbat, J. H. Freed, *J. Magn. Reson.* **2005**, *172*(2), 279–295.
- [57] G. Jeschke, V. Chechik, P. Ionita, A. Godt, H. Zimmermann, J. Banham, C. R. Timmel, D. Hilger, H. Jung, *Appl. Magn. Reson.* **2006**, *30*(3–4), 473–498.
- [58] K. Liebl, T. Drsata, F. Lankas, J. Lipfert, M. Zacharias, *Nucleic Acids Res.* **2015**, *43*(21), 10143–10156.
- [59] T. E. Edwards, P. Cekan, G. W. Reginsson, S. A. Shelke, A. R. Ferré-D'Amaré, O. Schiemann, S. T. Sigurdsson, *Nucleic Acids Res.* **2011**, *39*(10), 4419–4426.
- [60] J. E. Banham, C. M. Baker, S. Ceola, I. J. Day, G. H. Grant, E. J. J. Groenen, C. T. Rodgers, G. Jeschke, C. R. Timmel, *J. Magn. Reson.* **2008**, *191*(2), 202–218.
- [61] A. Marko, D. Margraf, H. Yu, Y. Mu, G. Stock, T. Prisner, *J. Chem. Phys.* **2009**, *130*(6).
- [62] A. Marko, D. Margraf, P. Cekan, S. T. Sigurdsson, O. Schiemann, T. F. Prisner, *Phys. Rev. E - Stat. Nonlinear, Soft Matter Phys.* **2010**, *81*(2), 1–9.
- [63] T. F. Prisner, A. Marko, S. T. Sigurdsson, *J. Magn. Reson.* **2015**, *252*, 187–198.
- [64] X. J. Lu, W. K. Olson, *Nucleic Acids Res.* **2003**, *31*(17), 5108–5121.
- [65] R. Kumar, H. Grubmüller, *Bioinformatics* **2015**, *31*(15), 2583–2585.
- [66] I. Beššeová, P. Banáš, P. Kührová, P. Košinová, M. Otyepka, J. Šponer, *J. Phys. Chem. B* **2012**, *116*(33), 9899–9916.

Manuscript received: February 3, 2024

Accepted manuscript online: March 26, 2024

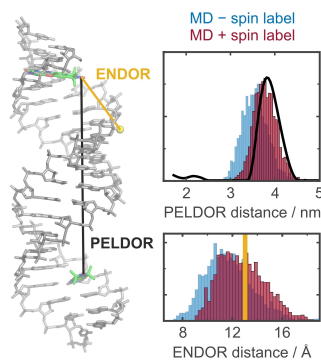
Version of record online: ■■■, ■■■

## Research Articles

## Biomolecular Chemistry

M. Gauger, M. Heinz, A.-L. J. Halbritter,  
L. S. Stelzl, N. Erlenbach, G. Hummer,\*  
S. T. Sigurdsson,\*  
T. F. Prisner\* \_\_\_\_\_ e202402498

Structure and Internal Dynamics of Short  
RNA Duplexes Determined by a Combina-  
tion of Pulsed EPR Methods and MD  
Simulations



We combined orientation-selective PELDOR and  $^{19}\text{F}$  Mims ENDOR to characterize the structural ensemble of RNA duplexes and their internal motions. In a quantitative comparison to MD simulations of RNA with and without spin labels, we found that state-of-the-art force fields with explicit parameterization of the spin label can describe the conformational ensemble present in our experiments.